STRUCTURAL CHEMISTRY

ISSN 2053-2296

Occupational modulation in the (3+1)-dimensional incommensurate structure of (2*S*,3*S*)-2-amino-3-hydroxy-3-methyl-4-phenoxybutanoic acid dihydrate

Kyana M. Sanders,[a] Samantha K. Bruffy,[a] Andrew R. Buller,[a] Václav Petříček[b] and Ilia A. Guzei[a]*

[a]Department of Chemistry, University of Wisconsin-Madison, 1101 University Ave, Madison, WI 53706, USA, and [b]Department of Structure Analysis, Institute of Physics of the Czech Academy of Sciences, Na Slovance 2, 182 00 Prague 8, Czech Republic. *Correspondence e-mail: iguzei@chem.wisc.edu

Received 20 May 2024
Accepted 17 July 2024

Edited by R. I. Cooper, University of Oxford, United Kingdom

Keywords: crystal structure; modulated structure; incommensurate modulation; supercell approximation; occupational/positional disorder; hydrogen bonding.

B-IncStrDB reference: 13272ESbhTu

CCDC references: 2371542; 2371541; 2371540; 2371539

Supporting information: this article has supporting information at journals.iucr.org/c

The incommensurately modulated structure of (2*S*,3*S*)-2-amino-3-hydroxy-3-methyl-4-phenoxybutanoic acid dihydrate ($C_{11}H_{15}NO_4{\cdot}2H_2O$ or **I**·$2H_2O$) is described in the (3+1)-dimensional superspace group $P2_12_12_1(0\beta0)000$ (β = 0.357). The loss of the three-dimensional periodicity is ascribed to the occupational modulation of one positionally disordered solvent water molecule, where the two positions are related by a small translation [*ca* 0.666 (9) Å] and ∼168 (5)° rotation about one of its O—H bonds, with an average 0.624 (3):0.376 (3) occupancy ratio. The occupational modulation of this molecule arises due to the competition between the different hydrogen-bonding motifs associated with each position. The structure can be very well refined in the average approximation (all satellite reflections disregarded) in the space group $P2_12_12_1$, with the water molecule refined as disordered over two positions in a 0.625 (16):0.375 (16) ratio. The refinement in the commensurate threefold supercell approximation in the space group $P112_1$ is also of high quality, with the six corresponding water molecules exhibiting three different occupancy ratios averaging 0.635:0.365.

1. Introduction

The implementation of enzymes in industry has advanced the synthesis of pharmaceuticals and bioactive compounds. Still, the use of enzymes is dwarfed in comparison to the plethora of established organic transformations. In particular, successful examples of enzyme-catalyzed C—C bond formation reactions with simple C-nucleophiles and C-electrophiles are limited. The Buller Lab has recently characterized an L-threonine transaldolase, ObiH, which generates a high-energy carbanion intermediate that is shielded from protonation (Kumar *et al.*, 2021; Doyon *et al.*, 2022). Natively, the nucleophilic intermediate intercepts a phenylacetaldehyde electrophile enantioselectively, producing the β-OH amino acid (2*S*,3*R*)-2-amino-3-hydroxy-4-(4-nitrophenyl)butanoic acid, an intermediate in obafluorin biosynthesis (Schaffer *et al.*, 2017; Scott *et al.*, 2017). It was hypothesized that the kinetically trapped intermediate of ObiH may enable productive catalysis with even less reactive electrophiles, such as ketones, generating tertiary β-OH amino acid. Such tertiary alcohols are a common motif in bioactive molecules, but their enantioselective synthesis is a long-standing challenge in both traditional synthetic chemistry and biocatalysis. Phenoxypropan-2-one was selected as a substrate for the ObiH reaction to explore nonnative aldol addition activity to make a tertiary alcohol.

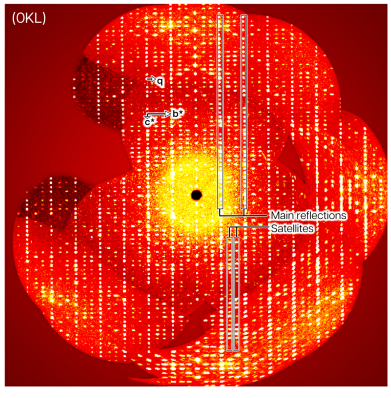

Table 1
Crystallographic experimental details.

	I·2H$_2$O(av)	**I**·2H$_2$O(NS2)	**I**·2H$_2$O(supercell)	**I**·2H$_2$O(mod)
Crystal data				
M_r	261.27	261.28	261.27	261.3
Crystal system, space group		Orthorhombic, $P2_12_12_1$	Monoclinic, $P112_1$	Orthorhombic, $P2_12_12_1(0\beta0)000$ β = 0.357
a, b, c (Å)		5.6620 (5), 6.3235 (5), 35.277 (3)	5.6737 (11), 19.021 (4), 35.298 (7)	5.662 (2), 6.324 (2), 35.276 (7)
γ (°)			90.030 (7)	
V (Å^3)		1263.05 (18)	3809.4 (12)	1263.1 (6)
Z		4	12	4
Radiation type			Cu $K\alpha$	
Temperature (K)			100	
μ (mm^{-1})			0.95	
Crystal size (mm)			0.18 × 0.16 × 0.11	
Data collection				
T_{min}, T_{max}		0.674, 0.754	0.678, 0.754	0.678, 0.754
No. of measured, independent, and observed reflections		24427, 2563, 2552 [$I > 2\sigma(I)$]	84909, 15929, 14589 [$I > 2\sigma(I)$]	28094, 7937, 7346 [$I > 3\sigma(I)$]
R_{int}		0.026	0.049	0.028
(sin $\theta/\lambda)_{max}$ (Å^{-1})			0.633	
Refinement				
$R[F^2 > 2\sigma(F^2)]$, $wR(F^2)$, S	0.025, 0.068, 1.08	0.012, 0.030, 1.12	0.053, 0.158, 1.07	0.0364, 0.0956, 2.203
No. of reflections	2563	2563	15929	7937
No. of parameters	204	362	1055	574
No. of restraints	6	24	5	13
H-atom treatment	H atoms treated by a mixture of independent and constrained refinement	All H-atom parameters refined	All H-atom parameters constrained	H atoms treated by a mixture of independent and constrained refinement
$\Delta\rho_{max}$, $\Delta\rho_{min}$ (e Å^{-3})	0.23, −0.15	0.19, −0.11	0.55, −0.39	0.24, −0.16
Absolute structure	Flack x determined using 1015 quotients $[(I^+) - (I^-)]/[(I^+) + (I^-)]$ (Parsons *et al.*, 2013)	Hooft *et al.* (2010)	Flack x determined using 6275 quotients $[(I^+) - (I^-)]/[(I^+) + (I^-)]$ (Parsons *et al.*, 2013)	3363 of Friedel pairs used in the refinement
Absolute structure parameter	0.02 (3)	0.03 (2)	0.03 (6)	0.03 (8)

For all determinations: $C_{11}H_{15}NO_4$·2H$_2$O. Experiments were carried out at 100 K using a Bruker D8 VENTURE diffractometer. Absorption was corrected for by multi-scan methods (*SADABS*; Krause *et al.*, 2015). Computer programs: *APEX3* (Bruker, 2019), *SAINT-Plus* (Bruker, 2019, 2020), *SHELXT* (Sheldrick, 2015*a*), *SHELXL* (Sheldrick, 2015*b*), *OLEX2* (Dolomanov *et al.*, 2009), and *JANA2020* (Petříček *et al.*, 2023).

Analytical reactions showed evidence of good conversion (>10 000 turnover number; Kozuch & Martin, 2012), albeit with low diastereoselectivity compared to that of aldehyde substrates. To determine the preferred relative stereoselectivity for the enzymatic addition into the ketone and understand how the selectivity compares to that with aldehyde substrates, (2*S*,3*S*)-2-amino-3-hydroxy-3-methyl-4-phenoxybutanoic acid (**I**·2H$_2$O) was isolated and characterized by small-molecule crystallography.

I·2H$_2$O is an example of a structure that can be equally well refined with and without taking the satellite reflections into account. The average structure model that disregards the satellite peaks meets all structural validation criteria (Spek, 2020) and refines without any indication of structural deficiencies. So does the structural model in the threefold supercell approximation. The refinement in superspace is also of good quality. The structure solution and refinement techniques of modulated structures are well established (de Wolff *et al.*, 1974, 1977; Janner & Janssen, 1977; van Smaalen *et al.*, 1995, 2004; Yamamoto, 1996; Wagner & Schönleber, 2009; Janssen, 2012; Schönleber, 2023), and are typically performed with *SUPERFLIP* (Palatinus & Chapuis, 2007), *SHELXT* (Sheldrick, 2015*a*), and *JANA* (Petříček *et al.*, 2014, 2016, 2023). The number of reported modulated organic structures has been growing (Schönleber, 2011, 2023; Pinheiro & Abakumov, 2015; Brock, 2016) and in order to find other examples of structures that can be described well with all three approaches, we interrogated the following two databases. A manual survey of the Bilbao Incommensurate Structures Database (Aroyo *et al.*, 2006), containing 263 structures as of March 15, 2024, resulted in 23 reports of incommensurately modulated organic structures. A search of the Cambridge Structural Database (CSD; Allen, 2002; Groom & Allen, 2014; Groom *et al.*, 2016) for 'modulated, organic only, 3D coordinates determined' structures resulted in 11 hits. A personal correspondence with a CSD representative disclosed that whereas modulated structure entries may not be marked well and may be difficult to find, addressing this issue is on the CSD's radar. Ultimately, it was not possible to find similar examples in the literature, but they must undoubtedly exist; numerous colleagues suggested that in the olden days of point detectors satellite reflections were likely missed, yet those

structures were established and published, but the evidence seems to be anecdotal. The authors reporting modulated structures consider the average and/or supercell approximate structures when appropriate, but seldom report all three and at least one of them is usually problematic.

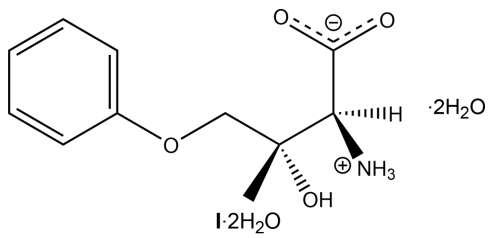

I·2H$_2$O
Scheme 1

A CSD search for hydrated zwitterions relevant to **I** identified 31 compounds among which 10 compounds contained solvent water in the lattice and two had $Z' \geq 3$. In all 10 structures, hydrogen-bonding interactions play an important role, but none of them is modulated. The two higher Z' compounds are 2-ammonio-3-hydroxy-2-(hydroxymethyl)-5-phenylpentanoate (Z' = 3; Hernandez *et al.*, 2015) and ammonium *O*-phospho-L-threonine hydrate (Z' = 4; Bryndal *et al.*, 2003). Both crystallize in Sohncke groups; in each, the symmetry-independent zwitterions exhibit different conformations and are not related by pseudosymmetry. An evaluation of the Bilbao database for incommensurate structures containing a hydrate results in several examples of incommensurate metal–organic complexes (Evain *et al.*, 2006; Cepeda *et al.*, 2012; Bednarchuk *et al.*, 2019; Gil-García *et al.*, 2023), but only one example of an organic compound where water is present as a solvent of crystallization (Rekis *et al.*, 2020, 2021). The latter article describes a superspace structure of sodium saccharinate 1.875-hydrate, in which the water molecules are believed to be space filling. In contrast, the water molecules in the structure presented herein play the dominant role.

The goal of the present article is to report an example of an incommensurately modulated structure that can be equally well characterized by applying the (3+1)-dimensional superspace approach, as well as average structure and supercell approximations. The occupational modulation of the positionally disordered solvent water molecule in the structure of **I**·2H$_2$O results from the competition between the two hydrogen-bonding motifs that correspond to each disorder position, which are related by a small ∼0.666 (9) Å translation and ∼168 (5)° rotation about one of its O—H bonds.

2. Experimental

2.1. Single-crystal X-ray diffraction

The crystal evaluation and data collection (Table 1) were performed on a Bruker D8 Venture PHOTON III four-circle diffractometer with Cu $K\alpha$ (λ = 1.54178 Å) radiation and a detector-to-crystal distance of 5.0 cm at 100 K. The unit-cell constants for the average structure and modulated structure with one **q** vector (β = 0.357) were refined with an automated routine built into the *APEX3* program (Bruker, 2019). The data were collected using the full sphere data collection routine to survey the reciprocal space to a resolution of 0.80 Å. A total of 24 427 data were harvested by collecting 19 sets of frames with 1° scans in ω and φ, with an exposure time 1–10 s per frame. These highly redundant data sets were corrected for Lorentz and polarization effects. The absorption correction was based on fitting a function to the empirical transmission surface as sampled by multiple equivalent measurements (Krause *et al.*, 2015).

A crystal of **I**·2H$_2$O was used for unit-cell determination at different temperatures in the 100–293 K range in order to detect a different unmodulated phase, but no other unit cell was discovered.

2.2. Refinement of the average structure

A successful solution of the average structure based only on the main reflections in the space group $P2_12_12_1$ by intrinsic phasing provided most non-H atoms from the *E* map. The remaining non-H atoms were located in an alternating series of least-squares cycles and difference Fourier maps. All non-H atoms were refined with anisotropic displacement coefficients. All H atoms attached to C atoms were included in the structure-factor calculations at idealized positions and were allowed to ride on the neighboring atoms with relative isotropic displacement coefficients.

The compound cocrystallizes with two solvent water molecules. The O6 water molecule is disordered over two positions, with a major component contribution of 0.625 (16). Both disorder components for this water molecule were refined with geometrical distance restraints (Guzei, 2014). All 10 hydrogen-bond donors and acceptors in the structure participate in intermolecular hydrogen-bonding interactions. The absolute structure was unequivocally established by anomalous dispersion effects. The absolute configuration of both chiral atoms C2 and C3 is *S*. Visualization of the average structure and the resulting Fourier electron-density maps was done with the *OLEX2* software package (Dolomanov *et al.*, 2009).

2.3. *NoSpherA2* refinement of the average structure

A second refinement of the average structure, using nonspherical atomic form factors, was performed using the *NoSpherA2* extension of the *olex2.refine* program (Bourhis *et al.*, 2015; Kleemiss *et al.*, 2021). The nonspherical atomic structure factors were determined by density functional theory (DFT) calculations (Neese, 2012, 2018), using the B3LYP hybrid functional and the def2-SVP basis set. All atoms were refined with anisotropic displacement coefficients. Both components for the disordered water molecule were refined with geometrical (Guzei, 2014) and atomic displacement parameter restraints.

2.4. Supercell refinement of the 1×3×1 commensurate approximate structure

Data integration and reduction were conducted in a routine fashion typical for 3D-periodic single-crystal data and only the

first-order satellites were observed and taken into consideration for the supercell refinement. Due to the closeness of the **q**-vector component $\beta = 0.357$ to 1/3, indexing the reflections for a $1\times3\times1$ supercell with a tripled b axis and tripled unit-cell volume of the basic cell was logical. However, generation of the supercell lowers the crystal symmetry from orthorhombic to monoclinic as the twofold screw operation along the b axis is lost during the conversion and now either the a or c axis could be chosen as unique. A refinement with the c axis unique produced better residuals and was chosen for the final supercell model in the space group $P112_1$. *JANA2020* (Petříček *et al.*, 2023) was used to generate the molecular coordinates for the supercell structure based on a $1\times3\times1$ approximate of the superspace model.

All non-H atoms were refined with anisotropic displacement coefficients. All H atoms attached to C atoms were included in the structure-factor calculations at idealized positions and were allowed to ride on the neighboring atoms with relative isotropic displacement coefficients. All six O atoms corresponding to the disordered water molecule in the average structure were refined with atomic displacement-parameter constraints. All water molecules were refined with geometrical constraints (Guzei, 2014).

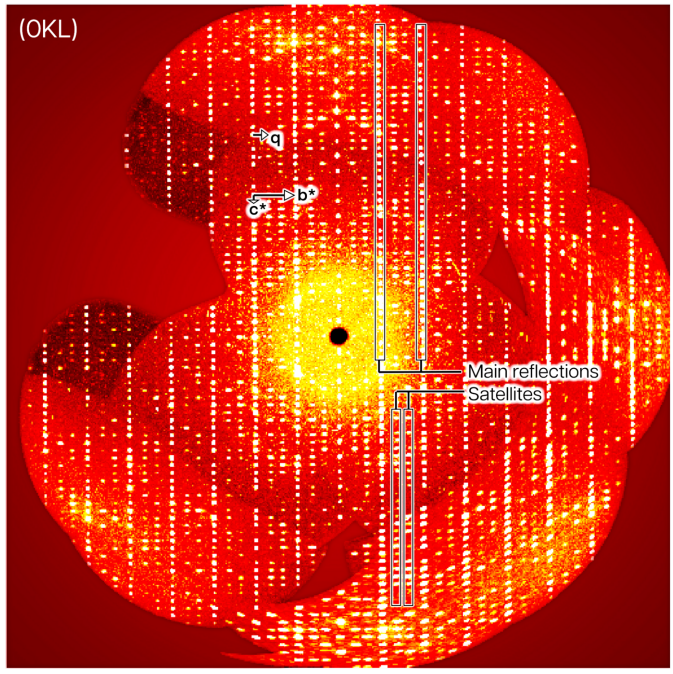

Figure 1
Annotated reconstruction of the 0*kl* reciprocal space layer for **I**·2H_2O(mod).

2.5. Superspace refinement of the (3+1)D incommensurately modulated structure

The atomic coordinates from the average structure refinement were imported into *JANA2020* (Petříček *et al.*, 2023) in preparation for the superspace refinement of the (3+1)-dimensional structure. At the start of the refinement process, the structure was refined on F^2 in the superspace group $P2_12_12_1(0\beta0)000$ ($\beta = 0.357$) using only the main reflections to establish a baseline 'average' structure refinement following importation into *JANA2020*. Once the modulation wave parameters were introduced to the model, both satellite and main reflections were taken into consideration and the instability factor was calculated from the reflection statistics. The average structure could also be solved independently with either *SUPERFLIP* (Palatinus & Chapuis, 2007) or *SHELXT* (Sheldrick, 2015*a*) within *JANA2020* in a straightforward manner.

The structure was refined as an inversion twin, with a minor component contribution of 3(8)%. All non-H atoms were refined with anisotropic displacement coefficients, while all carbon-bound H atoms were placed in idealized positions and allowed to ride on neighboring atoms with relative isotropic displacement coefficients. The remaining H atoms (those bound to N or O atoms) were refined with geometric and atomic displacement-parameter restraints in a manner consistent with the *SHELXL* refinement of the average structure. Unlike the average structure refinement, however, both ordered and disordered water molecule geometries were restrained based on a DFT-optimized geometry (Guzei, 2014).

The displacive modulation for all atoms in the zwitterion and the ordered O5 water molecule was described with one harmonic modulation wave and the anisotropic displacement parameter (ADP) modulation for the non-H atoms in these molecules was also described with one harmonic modulation wave. The refinement of the occupational and positional modulations of the disordered water molecule (the major disorder component is labeled O6 and the minor O7) was problematic and several models were explored (see next paragraph). The best superspace refinement results from a model where the O6 and O7 water molecules are treated as rigid bodies (centered on the O atoms), the occupational modulation is described with a second-order harmonic function (where the occupancy modulation of the major and minor disorder components is constrained to be complementary), and the positional modulation is described with a first-order harmonic function. All attempts to model the ADP modulation of atoms O6 and O7 resulted in nonpositive-definite U^{ij} tensors; thus, these atoms were refined without ADP modulation. Visualization of the modulated structure and the associated Fourier electron-density map was performed using the *JanaDraw* and *RunContour* extensions in *JANA2020* (Petříček *et al.*, 2023), respectively.

Additional refinement details: The rigid-body approach for the refinement of the disordered water molecule was deemed necessary because the displacive modulations of the riding H atoms could not be reliably refined independently. Refinement of the occupancy modulation using only first-order harmonics resulted in unrealistic values (up to 112% for O6 and as low as −12% for O7; see Fig. S2 in the supporting information); thus, we turned to a refinement where the first and second-order satellites were treated as overlapped reflections, allowing for the implementation of a second-order harmonic function for the occupancy modulation of the disordered water molecules.

However, attempts to refine the positional modulation for either the ordered or disordered atoms with second-order harmonics led to instabilities in the refinement, likely due to the comparatively weak contribution of the displacive modulation component to the overall behavior of the structure; thus, the use of a first-order harmonic was considered sufficient.

Refinement of the occupational modulation of the disordered water molecule with a crenel function was also explored. The magnitude of delta corresponding to the average occupancy of the O6 atom refined to a value of 0.6659, which is slightly larger than those resulting from the refinement of the average structure in *SHELXL* (0.625) and *JANA* (0.631). Indeed, visualization of this discontinuous occupancy function for atom O6 over an interval of t and overlayed with the electron-density map clearly reveals this value to be an overestimation of the occupancy of the O6 molecule (Fig. S1). A refinement where the delta value for the water molecule containing atom O6 was constrained to be equal to the occupancy value of the O6 atom in the refinement of the average structure in *JANA* was considered, but it was decided that such an approach was not satisfying or well justified.

2.6. Density functional theory (DFT) calculations

The geometry of **I** was optimized with *GAUSSIAN16* (Frisch *et al.*, 2016) at the B3LYP/6-311+G(d,p) level of theory with the polarizable continuum model for implicit aqueous solvation.

2.7. Synthetic procedure

The synthetic procedure is reported by Bruffy *et al.* (2023).

3. Structure solution and refinement

The diffraction pattern (Fig. 1) clearly shows the presence of strong main and weaker satellite reflections (Table 2). The reflections were indexed for three different refinement models as follows: (i) with three *hkl* Miller indices considering the main reflections only for the average structure solution and refinement; (ii) with three Miller indices only in the superstructure (V = 3787 Å^3) that is based on both main and satellite reflections; (iii) with three *hkl* Miller indices and one **q**-vector in the superspace model based on the main and first-order satellite reflections.

3.1. Average structure I·2H$_2$O(av)

The zwitterion **I** crystallizes with a proton transferred from the carboxyl group to amine atom N1 and two water solvent molecules in the asymmetric unit (Fig. 2). The absolute structure [Hooft y = 0.02 (3)] and absolute configuration (*S* for both C2 and C3) were unequivocally established by resonant scattering effects. All bond distances and interatomic bond angles fall in the usual ranges, as confirmed by a *Mogul* (Bruno *et al.*, 2004) geometry check, with a possible exception of the carboxylate atoms O1, O2, and C1 being coplanar with atoms N1 and C2 within 0.027 Å. The arene ring and atom O4 are coplanar within 0.015 Å, but atoms C3 and C5 are displaced by 0.26 (5) Å from this plane. One water molecule (O5) is fully occupied and ordered, whereas the other is disordered over positions O6 and O7 in a 0.625 (16):0.375 (16) ratio.

Table 2
Average intensities of the main and satellite reflections for I·2H$_2$O(mod) with respect to the supercell index m.

Miller index	<I>	<I/σ>
m (main reflection)	238.81	33.96
m − 1 (satellite reflection)	16.22	12.06
m + 1 (satellite reflection)	16.12	12.09

There are five hydrogen-bond donor atoms with 10 H atoms among them; all ten H atoms participate in intermolecular hydrogen-bonding interactions. These bonds are of the types O—H···O and N—H···O, and range from weak to strong and charge-assisted, with D—H···A distances ranging between 2.7071 (17) and 3.0237 (18) Å, with the D—H···A angles falling in the 139 (5)–173 (2)° range. The important part of the hydrogen-bonding network involves the ammonium N1 atom and both water molecules. The ammonium group forms a bond to the disordered water molecule (either N1—H1C···O6 or N1—H1C···O7), which in turn makes a hydrogen-bonding interaction with one of its H atoms with the ordered O5 water molecule (O6—H6B···O5 and O7—H7B···O5). However, the other H atoms on each partially occupied water molecule point in the opposite directions and form bonds to two different ordered water molecules: the higher populated site O6 forms the stronger bond O6—H6A···O5($x + \frac{1}{2}$, $-y + \frac{3}{2}$, $-z + 1$), with D···A = 2.980 (7) Å and D—H···A = 154 (3)°, whereas the less populated site is characterized with a shorter O7—H7A···O5($x - \frac{1}{2}$, $-y + \frac{3}{2}$, $-z + 1$) distance of D···A = 2.849 (12) Å and a suboptimal D—H···A angle of 139 (5)° (Fig. 3). The hydrogen bonds form ∼7.2 Å-thick two-dimensional networks parallel to the *ab* plane and are separated by hydrophobic layers along the *c* direction.

The hydrogen-bonding interactions are shown in Fig. 4, similar to the approach of Savic *et al.* (2021). The molecules of **I** are linked into hydrogen-bonded columns along the *a*

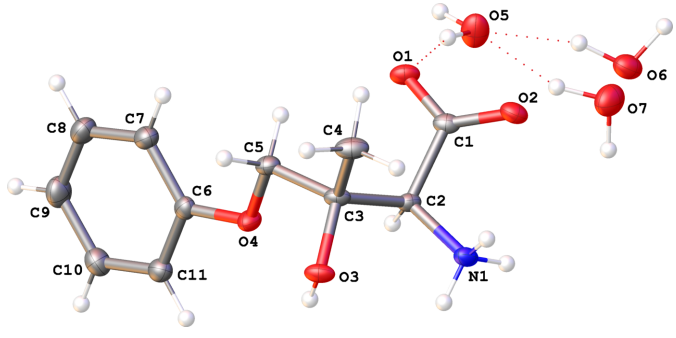

Figure 2
Molecular drawing of the asymmetric unit of the average structure **I**·2H$_2$O(av), shown with 50% probability displacement ellipsoids. The O6 water molecule is present 62.5 (16)% of the time and the O7 water molecule 37.5 (16)% of the time. The configuration of both chiral atoms C2 and C3 is *S*.

direction by an $R_2^2(8)$ motif N1→O2···O1←O3, which is seen in each column of molecules in Fig. 3. Each column is connected to a column related by 2_1 with hydrogen-bonding $R_3^2(9)$ motifs N1→O2←N1···O2←N1, observed between the molecular columns in Fig. 3; these columnar dimers propagate in the *a* direction. The columnar dimers are connected in the *b* direction by solvent water molecules into two-dimensional sheets perpendicular to *c* as follows. The water molecules O5 connect two columns of **I** related by a 1,0,0 translation into dimeric columns along *b* with a $C_3^3(6)$ motif O1←O5→O3→O1. In Fig. 4, these interactions appear as O1←O5→O3→O1 triangles, but they are spirals because the O5 atoms connect molecules in different layers perpendicular to the plane of the paper (*b* direction) rather than in the plane of the paper. The water molecules O6 form three hydrogen bonds and so do the molecules of O7 (Fig. 4). Two of their interactions are to the same atoms, O6→O5 and O6←N1, and O7→O5 and O7←N1, correspondingly. Their third bonds differ, O6→O5′ *versus* O7→O5″, and are shown in red to emphasize the difference. At this point, further graph-set notation descriptions of the hydrophobic layers parallel to the *ab* plane becomes impractical.

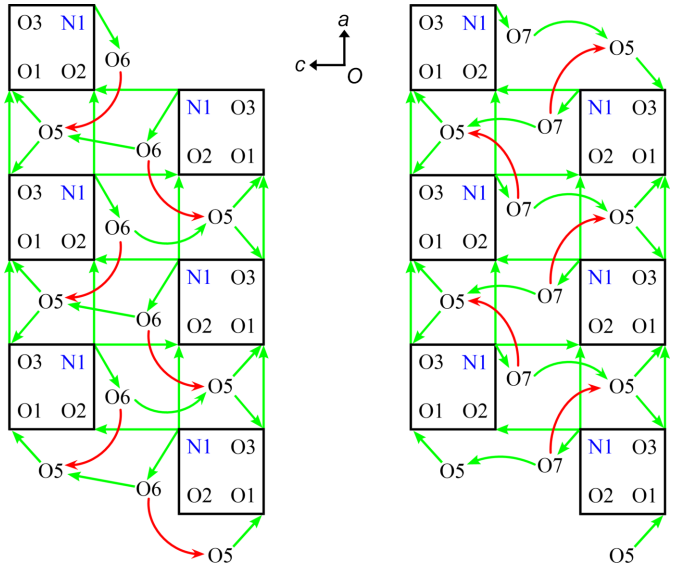

Figure 4
A schematic representation of hydrogen-bonding interactions in **I**·2H_2O(av). Each molecule of **I** is represented with a square with each corner marked with an atom label corresponding to a hydrogen bond donor (*D*) or acceptor (*A*). The arrows extend from *D*—H donors to acceptors: *D*→*A*.

3.2. Average structure refined with *NoSpherA2* **I**·2H_2O(NS2)

The structural refinement of the average structure with a nonspherical atom model, as implemented in the *NoSpherA2* extension of the *olex2.refine* program (Kleemiss *et al.*, 2021; Bourhis *et al.*, 2015), produces lower *R* factors and a more precise model with standard deviations on the interatomic bond distances two to three times smaller than those in **I**·2H_2O(av). These improvements come at the cost of a lower data-to-parameter ratio [7.08 for **I**·2H_2O(NS2) *versus* 12.6 for **I**·2H_2O(av)], as both non-H and H atoms are refined anisotropically. In **I**·2H_2O(NS2), the C—H and N—H distances are expectedly longer than the corresponding distances in **I**·2H_2O(av), but other distances show minor variations and the non-H-atom geometries of **I**·2H_2O(av) and **I**·2H_2O(NS2) can be superimposed with a root mean square deviation (RMSD) of 0.004 Å (Fig. 5).

3.3. Density functional theory (DFT) calculations (I-DFT)

The geometry of **I**-DFT closely matches the experimentally observed conformation; the non-H atoms of the molecule could be superimposed onto **I**·2H_2O(av), with RMSD =

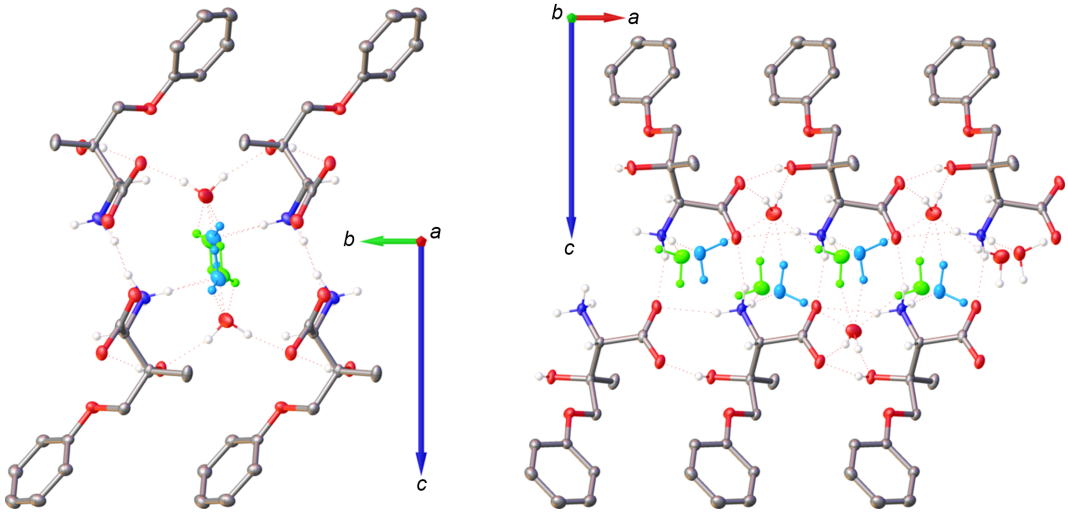

Figure 3
Molecular drawings highlighting the hydrogen-bonding network in the average structure **I**·2H_2O(av), shown along the *a* axis (left) and the *b* axis (right), with 50% probability displacement ellipsoids. The partially occupied O6 and O7 water molecules are shown in blue and green. All H atoms that do not participate in hydrogen-bonding interactions and are not bound to chiral atoms have been omitted.

Table 3
Occupancy factors of the water molecules at the six symmetry-independent sites in the supercell corresponding to the disordered water molecule (O6/O7) from the average structure.

Site	No suffix	*A*	*B*	*C*	*D*	*E*	Average
O6	0.654 (5)	0.248 (6)	1	0.654 (5)	0.254 (6)	1	0.635
O7	0.346 (5)	0.752 (6)	0	0.346 (5)	0.746 (6)	0	0.365

0.123 Å (Fig. 5). The main differences are in the relative orientations of the arene ring and carboxyl group: the dihedral angle between the arene planes in the superimposed **I**·2H_2O(av) and **I**-DFT is 8.8°, whereas the dihedral angle between the O1/O2/C1 planes measures 7.74°. In contrast to **I**·2H_2O(av), atoms C3 and C5 in **I**-DFT are nearly coplanar with the phenolate fragment.

A single-point energy calculation for the experimental geometry of **I**·2H_2O(NS2) reveals that its conformation is 9.8 kcal mol^{-1} higher than that of **I**-DFT. This may be in part due to suboptimal element–hydrogen distances, in part due to the omission of the water molecules, and in part due to lattice effects that stabilize the observed conformation of **I** that facilitates the formation of strong charge-assisted hydrogen bonds.

3.4. Supercell and superstructure model **I**·2H_2O(supercell)

Another approximation for the solid-state description of the incommensurately modulated **I**·2H_2O is the refinement of its superstructure in the supercell. Van Smaalen stated that a supercell refinement may be comparable to that of the superspace model when satellites of the first order only are taken into consideration (van Smaalen *et al.*, 1995). Indeed, this supercell approximation confirmed a strong occupational modulation of the disordered water molecules and a small positional modulation of both the zwitterion **I** and the ordered water molecule.

In the supercell approximation, the threefold lengthening of the *b* axis and lowering of the point-group symmetry from 222 to 2 resulted in $Z' = 6$ with six symmetry-independent molecules of **I** and 12 molecules of solvent water (Fig. 6). In the average structure, one water molecule is ordered and one disordered; therefore, in the supercell, the expectation was to observe six sites with ordered water molecules and six with disordered ones. This was not the case. The former six water molecules are ordered, but among the six sites for the latter six molecules, two contain ordered water molecules and four are occupied by disordered water molecules with two disorder ratios (Table 3). These differences in the occupational parameters must be the reason why the symmetry along the *b* axis is lost in the supercell.

These occupational percentages are explained with the help of Table 3 that lists them for the six sites of the expected disorder. The occupancies follow a sawtooth distribution both for O6 and for O7, with an average of 0.635 for the main disorder component. Whereas this number is in excellent agreement with the value of 0.625 (16) observed for **I**·2H_2O(av) and 0.624 (3) for **I**·2H_2O(mod), the individual occupancies at the six sites must be different in the crystal because the supercell refinement is an approximation due to the modulation wavelength being 2.8*b* (17.70 Å) rather than 3*b* (18.97 Å) exactly. It is instructive to compare the relative distribution of the occupancy factors of the disordered water molecules among **I**·2H_2O(av), **I**·2H_2O(supercell), and **I**·2H_2O(mod). Fig. 7 shows molecular arrangements along the *b* direction for the three models, but the disordered O6 and O7 molecules are shown only when their occupancy exceeds 50%

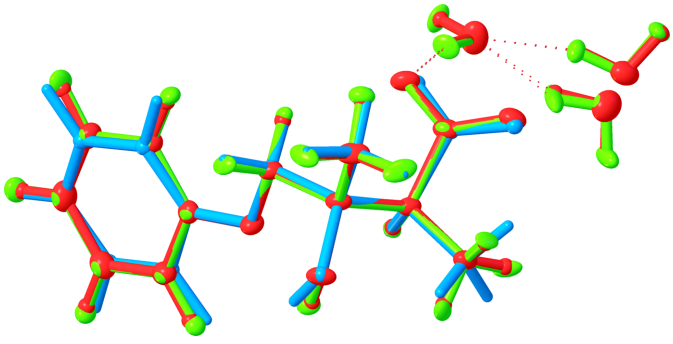

Figure 5
Overlay of **I**·2H_2O(av), **I**·2H_2O(NS2), and **I**-DFT shown in red, green, and blue, respectively.

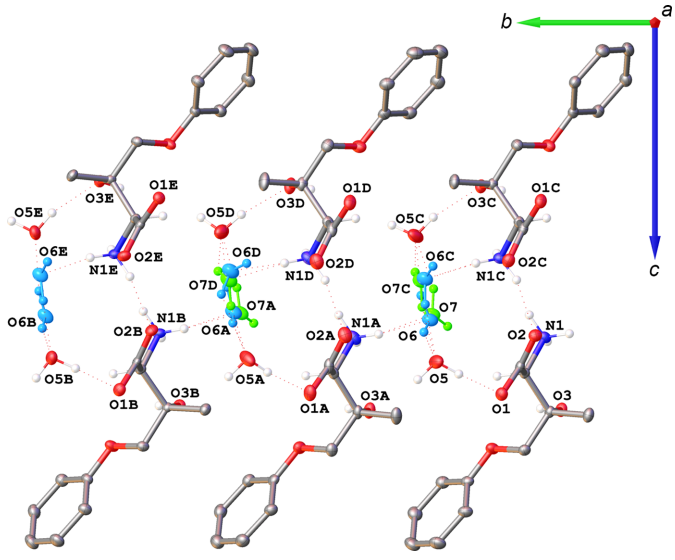

Figure 6
Molecular drawing of **I**·2H_2O(supercell), shown with 50% probability displacement ellipsoids. The six symmetry-independent sites in the supercell corresponding to the disordered O6 and O7 water molecules are shown in blue and green. All H atoms that do not participate in hydrogen-bonding interactions and are not bound to chiral atoms have been omitted.

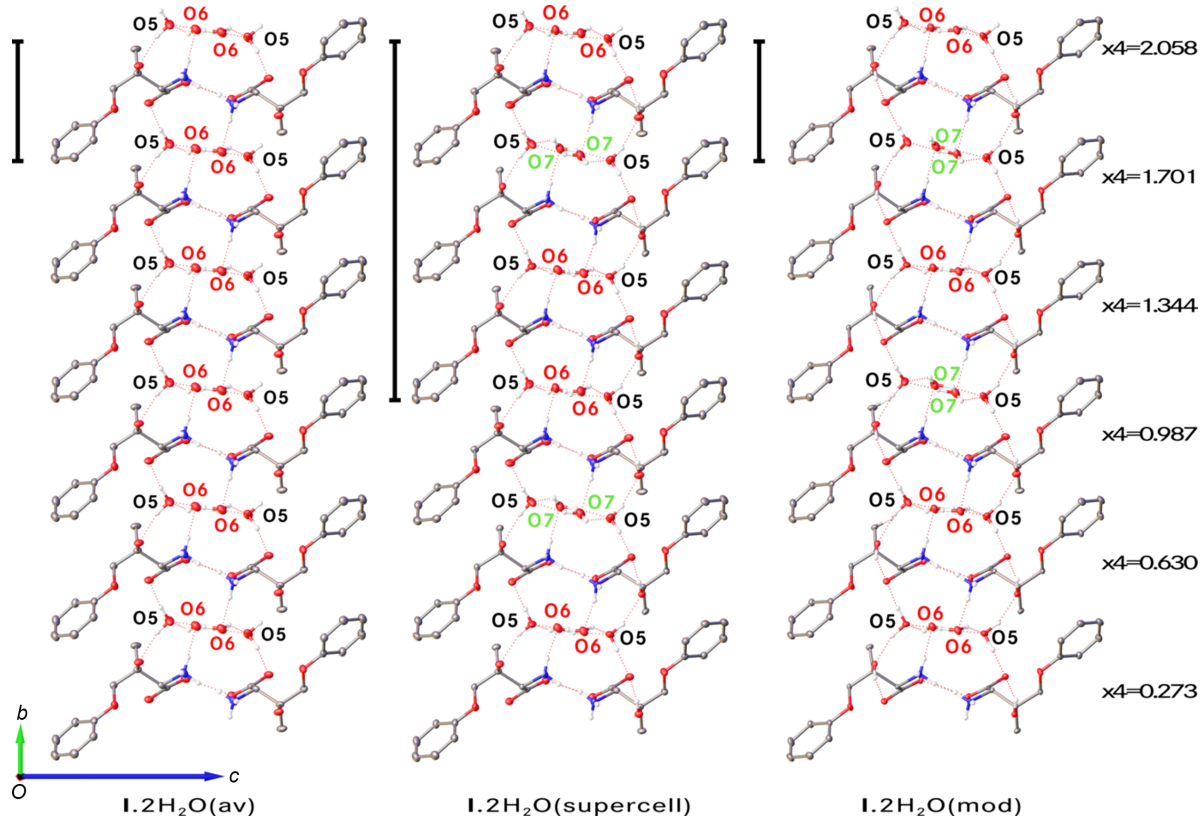

Figure 7
Molecular packing diagrams for **I**·2H_2O(av), **I**·2H_2O(supercell), and **I**·2H_2O(mod). Water molecules are shown if their occupancies exceed 50%. Only water molecules are labeled and all H atoms on C atoms have been omitted. The vertical bars represent the lengths of the *b* axes. For the **I**·2H_2O(mod), the t = 0 corresponds to the O6 atom coordinate y = 0.76343.

to demonstrate the differences in the modeled occupancy factors.

Fig. 8 highlights how viewing the six symmetry-independent molecules along the *b* direction gives an impression of the amplitude of the displacive modulation described with the superspace approach in Section 3.5. In the structure of **I**·2H_2O(supercell), the six molecules of **I** have very similar geometries: molecules with label suffixes *A*, *B*, *C*, *D*, and *E* can

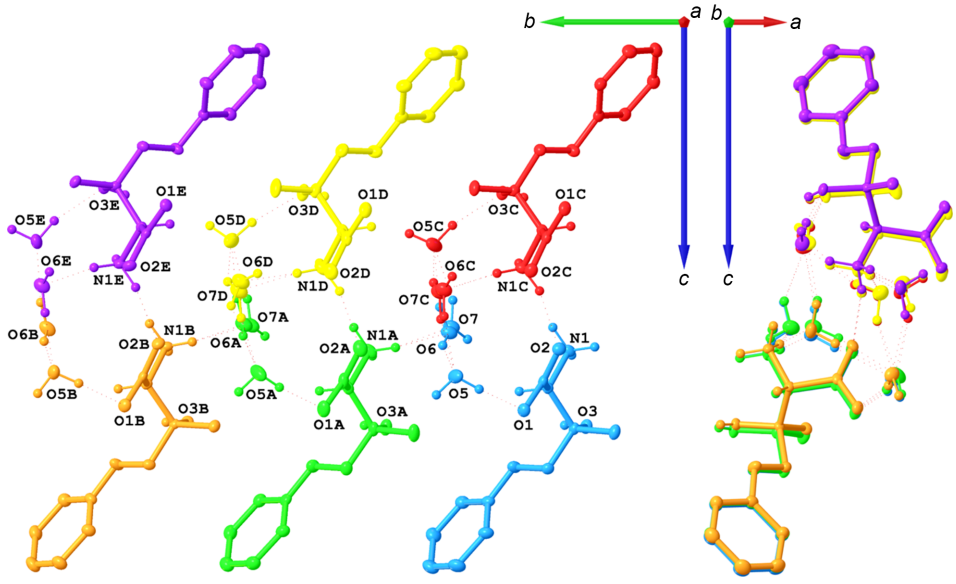

Figure 8
Molecular drawing of **I**·2H_2O(supercell), shown with 50% probability displacement ellipsoids along the *a* and *b* directions. The molecule without a label suffix is shown in blue, while the molecules with label suffixes *A*, *B*, *C*, *D*, and *E* are shown in green, orange, red, yellow, and purple, respectively. All H atoms that do not participate in hydrogen-bonding interactions and are not bound to chiral atoms have been omitted.

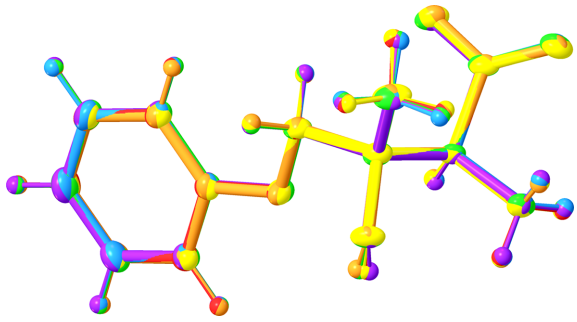

Figure 9
Overlay of the six symmetry-independent molecules of **I** in the structure of **I**·2H_2O(supercell), shown with 50% probability displacement ellipsoids. The molecules are matched by a least-squares fitting routine. The molecule without a label suffix is shown in blue, while the molecules with label suffixes *A*, *B*, *C*, *D*, and *E* are shown in green, orange, red, yellow, and purple, respectively.

each be superimposed (with the H atoms included) onto the molecule without a label suffix with RMSDs of 0.016, 0.053, 0.050, 0.057, and 0.037 Å, respectively (Fig. 9).

3.5. Superspace model **I**·2H_2O(mod)

The (3+1)D superspace approach is the most accurate way to describe the structure of **I**·2H_2O. Our final model, using two harmonic waves for the occupancy modulation of atoms O6 and O7 (Fig. 10), results in an average partial occupancy equal to 0.624 (3) for atom O6, which is nearly identical to the partial occupancy of O6 [0.625 (16)] obtained from the average structure refinement in *SHELXL*.

For the most part, the zwitterion moves as a rigid unit with a small displacement amplitude in the *a* and *b* directions, while in the *c* direction, all atoms move in a highly concerted fashion with a slightly larger degree of displacement, where the largest amplitude corresponds to the terminal C4 methyl group (∼0.15 Å). The exception occurs in the *b* direction, where the planar phenolate region exhibits a swaying motion corresponding to a 4.39 (11)° rotation of the arene ring about the O4—C6 bond. The amplitude of this motion (0.07 < dy < 0.12) is noticeably larger than that for the remaining regions of **I** in the *b* direction (where atom C5 has the largest amplitude of ∼0.05 Å). Atom N1 also exhibits a pronounced displacement amplitude in the *b* direction (∼0.08 Å), which likely results from the participation of the atom in hydrogen-bonding interactions. Plots showing the atomic displacement functions *versus t* for all non-H atoms are provided in Fig. S4 of the supporting information.

Overall, the amplitudes of the displacive modulation of **I**·2H_2O(mod) is small in all three directions (≤ 0.15 Å) and likely just a response to the occupational modulation of the disordered water molecule, which manifests itself as two orientations, with the O6—H6*B* and O7—H7*B* bonds pointing along the same direction in *c*, and the O6—H6*A* and O7—H7*A* bonds pointing in opposite directions along *a*. Neither orientation allows for perfectly optimized hydrogen-bonding interactions. In terms of the *D*···*A* distance, the O7 orientation appears to be favored over the O6 orientation [average *D*···*A* = 2.757 (19) Å *versus* 2.983 (4) Å for O7···O5^{v} and O6···O5^{iv}; symmetry codes: (iv) $x+\frac{1}{2}, -y+\frac{3}{2}, -z+1$; (v) $x-\frac{1}{2}, -y+\frac{3}{2}, -z+1$]. Meanwhile, in terms of the *D*—H···*A* angle, the O6 orientation appears to be favored [average *D*—H···*A* = 159 (4)° *versus* 140 (7)° for O6—H6*A*···O5^{iv} and O7—H7*A*···O5^{v}]. Thus, the occupational modulation likely arises from the competition between these hydrogen-bonding interactions. In fact, a plot of the occupational modulation *versus t* nicely aligns with how these hydrogen-bonding interactions fluctuate (Fig. 11). Specifically, the occupancy of O6 is lowest over the interval of 0.06 < *t* < 0.4, which is the same range during which the O6···O5^{iv} distance is the least optimized, while the occupancy of O7 is lowest over the interval of 0.6 < *t* < 0.9, which is the same range during which the O7—H7*B*···O5 and O7—H7*A*···O5^{v} angles are least optimized.

The N1^{iv}—H1*B*^{iv}···O6 and N1^{iv}—H1*B*^{iv}···O7 hydrogen-bond interactions follow a similar pattern, where the *D*···*A* distances are always slightly shorter for N1^{iv}···O7 than for N1^{iv}···O6 throughout the full range of *t* values, while the *D*—H···*A* angles for N1^{iv}—H1*B*^{iv}···O6 are better optimized compared to N1^{iv}—H1*B*^{iv}···O7 [170.8 (14)–173.8 (14) *versus* 159.7 (15)–169.6 (15)°] over the full range of *t* values. Speci-

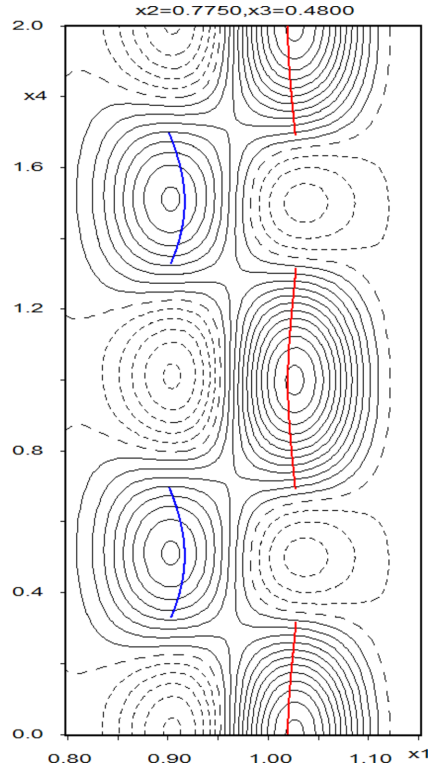

Figure 10
Electron-density plot showing the (3+1)D modulation of the O6 and O7 atoms along *x*1 as a function of *x*4, with the electron density summed over a thickness of 1 Å in the remaining directions. Solid and dashed black lines represent areas of positive and negative electron density. The curves of the red and blue lines represent the paths of motion of the O6 and O7 atoms. This occupational modulation is manifested as positional disorder where the water molecule is split over the O6 and O7 sites, which have an average occupancy ratio of 62.4 (3):37.6 (3) in **I**·2H_2O(mod).

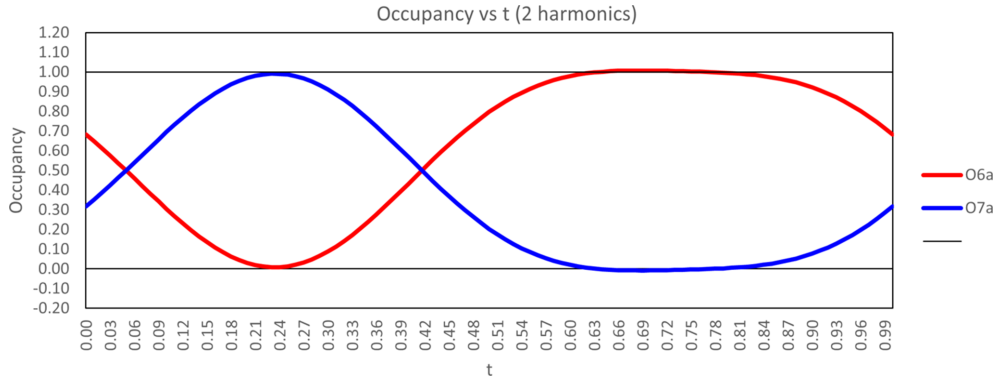

Figure 11
Plot of the two harmonic modulation functions used to model the occupancy modulation of atoms O6 and O7 *versus t*.

fically, the values for the N1$^{iv}\cdots$O6 and H1$B^{iv}\cdots$O6 distances, as well as the N1^{iv}—H1$B^{iv}\cdots$O6 angle, are the least optimized within the region of $0.06 < t < 0.4$ (where the occupancy of atom O6 approaches zero and the occupancy of atom O7 approaches 1), while the values for the H1$B^{iv}\cdots$O7 distance and the N1^{iv}—H1$B^{iv}\cdots$O7 angle are now the most optimized within the same range of t values. Plots showing the described hydrogen-bonding interactions *versus t* are provided in Figs. S5 and S6 of the supporting information.

The observed modulation emphasizes the role of hydrogen-bonding in the stabilization of the structure and is attributed to the occupational modulation of the disordered water molecule O6/O7. The intermolecular interactions formed by these partially occupied water molecules do not conform to the 3D space-group symmetry operations. Whereas a dynamical disorder between these two positions is possible due to the sufficient room in this void to allow, for example, molecule O6 to rotate about one of its O—H bonds and slide into the position of O7, it would be unlikely because there are no hydrogen-bond acceptors for the transition geometries of this molecule. Competition between the hydrogen bonding and preferred conformation of **I** does not seem to be a major reason because the geometry of **I** does not change with the modulation, but its orientation changes slightly. Interplay between the strong hydrogen bonding and optimal molecular packing may give rise to the loss of 3D symmetry, but again large displacive modulations in **I**·2H_2O(mod) are not observed. The molecules pack with alternating hydrogen-bonded hydrophilic and hydrophobic layers, with no π–π interactions in the lattice.

4. Conclusions

The average, commensurate supercell, and incommensurate superspace refinements provide adequate and comparable descriptions of **I**·2H_2O, but with varying levels of detail. In all three models, the disorder ratio for two positions of the disordered water molecule refines to essentially the same value, *i.e.* 0.63:0.37. The modulation in the superspace structure is characterized as moderate due to the strength of the first-order satellite reflections. The superspace refinement was problematic due to computational instabilities, occupational modulation, and possible satellite reflection overlap. The average structure provides a benchmark for the disorder refinement, and its high quality make it easy to overlook the modulation. An average structure refinement with non-spherical atom form factors did not uncover any structural problems. The supercell approximation reveals a more complicated nature of the positional disorder of the water molecule, and the superspace refinement clarifies the nature of the competition between the different hydrogen-bonding interactions of O6 and O7. There is a strong correlation between the behavior of the occupancy modulation of the positionally disordered O6/O7 water molecule and the optimization of the hydrogen-bonding motifs associated with each position.

Acknowledgements

The authors acknowledge Dr. Bruce Noll, Dr. Danielle L. Gray, and Dr. Daniel C. Fredrickson for helpful discussions regarding the superspace refinement.

Funding information

Funding for this research was provided by: National Science Foundation (grant No. CHE-1919350 to UW–Madison Department of Chemistry).

References

Allen, F. H. (2002). *Acta Cryst.* B**58**, 380–388.
Aroyo, M. I., Perez-Mato, J. M., Capillas, C., Kroumova, E., Ivantchev, S., Madariaga, G., Kirov, A. & Wondratschek, H. (2006). *Z. Kristallogr.* **221**, 15–27.
Bednarchuk, T. J., Hornfeck, W., Kinzhybalo, V., Zhou, Z., Dušek, M. & Pietraszko, A. (2019). *Acta Cryst.* B**75**, 1144–1151.
Bourhis, L. J., Dolomanov, O. V., Gildea, R. J., Howard, J. A. K. & Puschmann, H. (2015). *Acta Cryst.* A**71**, 59–75.
Brock, C. P. (2016). *Acta Cryst.* B**72**, 807–821.
Bruffy, S., Meza, A., Soler, J., Doyon, T., Young, S., Lim, J., Huseth, K., Garcia-Borràs, M. & Buller, A. (2023). *ChemRxiv*. doi: 10.26434/chemrxiv-2023-2v3cq.
Bruker (2019). *APEX3* and *SAINT-Plus*. Bruker AXS Inc., Madison, Wisconsin, USA.
Bruker (2020). *SAINT-Plus*. Bruker AXS Inc., Madison, Wisconsin, USA.

Bruno, I. J., Cole, J. C., Kessler, M., Luo, J., Motherwell, W. D. S., Purkis, L. H., Smith, B. R., Taylor, R., Cooper, R. I., Harris, S. E. & Orpen, A. G. (2004). *J. Chem. Inf. Comput. Sci.* **44**, 2133–2144.
Bryndal, I., Picur, B. & Lis, T. (2003). *J. Mol. Struct.* **647**, 295–310.
Cepeda, J., Balda, R., Beobide, G., Castillo, O., Fernández, J., Luque, A., Pérez-Yáñez, S. & Román, P. (2012). *Inorg. Chem.* **51**, 7875–7888.
Dolomanov, O. V., Bourhis, L. J., Gildea, R. J., Howard, J. A. K. & Puschmann, H. (2009). *J. Appl. Cryst.* **42**, 339–341.
Doyon, T. J., Kumar, P., Thein, S., Kim, M., Stitgen, A., Grieger, A. M., Madigan, C., Willoughby, P. H. & Buller, A. R. (2022). *ChemBioChem*, **23**, e202100577.
Evain, M., Petricek, V., Coué, V., Dessapt, R., Bujoli-Doeuff, M. & Jobic, S. (2006). *Acta Cryst.* B**62**, 790–797.
Frisch, M. J., Trucks, G. W., Schlegel, H. B., Scuseria, G. E., Robb, M. A., Cheeseman, J. R., Scalmani, G., Barone, V., Petersson, G. A., Nakatsuji, H., Li, X., Caricato, M., Marenich, A. V., Bloino, J., Janesko, B. G., Gomperts, R., Mennucci, B., Hratchian, H. P., Ortiz, J. V., Izmaylov, A. F., Sonnenberg, J. L., Williams, Ding, F., Lipparini, F., Egidi, F., Goings, J., Peng, B., Petrone, A., Henderson, T., Ranasinghe, D., Zakrzewski, V. G., Gao, J., Rega, N., Zheng, G., Liang, W., Hada, M., Ehara, M., Toyota, K., Fukuda, R., Hasegawa, J., Ishida, M., Nakajima, T., Honda, Y., Kitao, O., Nakai, H., Vreven, T., Throssell, K., Montgomery Jr., J. A., Peralta, J. E., Ogliaro, F., Bearpark, M. J., Heyd, J. J., Brothers, E. N., Kudin, K. N., Staroverov, V. N., Keith, T. A., Kobayashi, R., Normand, J., Raghavachari, K., Rendell, A. P., Burant, J. C., Iyengar, S. S., Tomasi, J., Cossi, M., Millam, J. M., Klene, M., Adamo, C., Cammi, R., Ochterski, J. W., Martin, R. L., Morokuma, K., Farkas, O., Foresman, J. B. & Fox, D. J. (2016). *GAUSSIAN16*. Revision C.01. Gaussian Inc., Wallingford, CT, USA. https://gaussian.com/.
Gil-García, R., Madariaga, G., Jiménez-Pérez, A., Herrán-Torres, I., Gago-González, A., Ugalde, M., Januskaitis, V., Barrera-García, J., Insausti, M. S., Galletero, M., Borrás, J., Cuevas, J. V., Pedrido, R., Gómez-Saiz, P., Lezama, L. & García-Tojal, J. (2023). *CrystEngComm*, **25**, 2213–2226.
Groom, C. R. & Allen, F. H. (2014). *Angew. Chem. Int. Ed.* **53**, 662–671.
Groom, C. R., Bruno, I. J., Lightfoot, M. P. & Ward, S. C. (2016). *Acta Cryst.* B**72**, 171–179.
Guzei, I. A. (2014). *J. Appl. Cryst.* **47**, 806–809.
Hernandez, K., Zelen, I., Petrillo, G., Usón, I., Wandtke, C. M., Bujons, J., Joglar, J., Parella, T. & Clapés, P. (2015). *Angew. Chem. Int. Ed.* **54**, 3013–3017.
Hooft, R. W. W., Straver, L. H. & Spek, A. L. (2010). *J. Appl. Cryst.* **43**, 665–668.
Janner, A. & Janssen, T. (1977). *Phys. Rev. B*, **15**, 643–658.
Janssen, T. (2012). *Acta Cryst.* A**68**, 667–674.
Kleemiss, F., Dolomanov, O. V., Bodensteiner, M., Peyerimhoff, N., Midgley, L., Bourhis, L. J., Genoni, A., Malaspina, L. A., Jayatilaka, D., Spencer, J. L., White, F., Grundkötter-Stock, B., Steinhauer, S., Lentz, D., Puschmann, H. & Grabowsky, S. (2021). *Chem. Sci.* **12**, 1675–1692.
Kozuch, S. & Martin, J. M. L. (2012). *ACS Catal.* **2**, 2787–2794.
Krause, L., Herbst-Irmer, R., Sheldrick, G. M. & Stalke, D. (2015). *J. Appl. Cryst.* **48**, 3–10.
Kumar, P., Meza, A., Ellis, J. M., Carlson, G. A., Bingman, C. A. & Buller, A. R. (2021). *ACS Chem. Biol.* **16**, 86–95.
Neese, F. (2012). *WIREs Comput. Mol. Sci.* **2**, 73–78.
Neese, F. (2018). *WIREs Comput. Mol. Sci.* **8**, e1327.
Palatinus, L. & Chapuis, G. (2007). *J. Appl. Cryst.* **40**, 786–790.
Parsons, S., Flack, H. D. & Wagner, T. (2013). *Acta Cryst.* B**69**, 249–259.
Petříček, V., Dušek, M. & Palatinus, L. (2014). *Z. Kristallogr.* **229**, 345–352.
Petříček, V., Eigner, V., Dušek, M. & Čejchan, A. (2016). *Z. Kristallogr.* **231**, 301–312.
Petříček, V., Palatinus, L., Plášil, J. & Dušek, M. (2023). *Z. Kristallogr.* **238**, 271–282.
Pinheiro, C. B. & Abakumov, A. M. (2015). *IUCrJ*, **2**, 137–154.
Rekis, T., Schaller, A. M., Kotla, S. R., Schönleber, A., Noohinejad, L., Tolkiehn, M., Paulmann, C. & van Smaalen, S. (2021). *IUCrJ*, **8**, 139–147.
Rekis, T., Schönleber, A. & van Smaalen, S. (2020). *Acta Cryst.* B**76**, 18–27.
Savic, V., Eder, F., Göb, C., Mihovilovic, M. D., Stanetty, C. & Stöger, B. (2021). *Acta Cryst.* B**77**, 83–92.
Schaffer, J. E., Reck, M. R., Prasad, N. K. & Wencewicz, T. A. (2017). *Nat. Chem. Biol.* **13**, 737–744.
Schönleber, A. (2011). *Z. Kristallogr.* **226**, 499–517.
Schönleber, A. (2023). *Phys. Sci. Rev.* **2023**, https://doi.org/10.1515/psr-2018-0140.
Scott, T. A., Heine, D., Qin, Z. & Wilkinson, B. (2017). *Nat. Commun.* **8**, 15935.
Sheldrick, G. M. (2015*a*). *Acta Cryst.* A**71**, 3–8.
Sheldrick, G. M. (2015*b*). *Acta Cryst.* C**71**, 3–8.
Smaalen, S. van (1995). *Crystallogr. Rev.* **4**, 79–202.
Smaalen, S. van (2004). *Z. Kristallogr.* **219**, 681–691.
Spek, A. L. (2020). *Acta Cryst.* E**76**, 1–11.
Wagner, T. & Schönleber, A. (2009). *Acta Cryst.* B**65**, 249–268.
Wolff, P. M. de (1974). *Acta Cryst.* A**30**, 777–785.
Wolff, P. M. de (1977). *Acta Cryst.* A**33**, 493–497.
Yamamoto, A. (1996). *Acta Cryst.* A**52**, 509–560.

supporting information

Acta Cryst. (2024). C**80** [https://doi.org/10.1107/S2053229624007009]

Occupational modulation in the (3+1)-dimensional incommensurate structure of (2*S*,3*S*)-2-amino-3-hydroxy-3-methyl-4-phenoxybutanoic acid dihydrate

Kyana M. Sanders, Samantha K. Bruffy, Andrew R. Buller, Václav Petříček and Ilia A. Guzei

Computing details

(buller05a_MOD)

Crystal data

$C_{11}H_{15}NO_4{\cdot}2(H_2O)$
M_r = 261.3
Orthorhombic, *P*212121(0β0)000†
q = 0.357270**b***
a = 5.662 (2) Å
b = 6.324 (2) Å
c = 35.276 (7) Å
V = 1263.1 (6) Å^3
Z = 4
F(000) = 560
D_x = 1.374 Mg m^{-3}
Cu *K*α radiation, λ = 1.54184 Å
μ = 0.95 mm^{-1}
T = 100 K
Block, colourless
0.18 × 0.16 × 0.11 mm

† Symmetry operations: (1) x_1, x_2, x_3, x_4; (2) $-x_1$+1/2, $-x_2$, x_3+1/2, $-x_4$; (3) $-x_1$, x_2+1/2, $-x_3$+1/2, x_4; (4) x_1+1/2, $-x_2$+1/2, $-x_3$, $-x_4$.

Data collection

Bruker D8 VENTURE diffractometer
Radiation source: X-ray tube
Multilayer mirror monochromator
Detector resolution: 7.41 pixels mm^{-1}
ω and φ scans
Absorption correction: multi-scan (SADABS; Krause *et al.*, 2015)
T_{min} = 0.678, T_{max} = 0.754
28094 measured reflections
7937 independent reflections
7346 reflections with $I > 3\sigma(I)$
R_{int} = 0.028
θ_{max} = 79.1°, θ_{min} = 2.8°
h = −7→7
k = −8→7
l = −44→44

Refinement

Refinement on F^2
$R[F > 3\sigma(F)]$ = 0.036
$wR(F)$ = 0.096
S = 2.20
7937 reflections
574 parameters
13 restraints
124 constraints
H atoms treated by a mixture of independent and constrained refinement
Weighting scheme based on measured s.u.'s $w = 1/(\sigma^2(I) + 0.000731I^2)$
$(\Delta/\sigma)_{max}$ = 0.016
$\Delta\rho_{max}$ = 0.24 e Å^{-3}
$\Delta\rho_{min}$ = −0.16 e Å^{-3}
Absolute structure: 3363 of Friedel pairs used in the refinement
Absolute structure parameter: 0.03 (8)

Fractional atomic coordinates and isotropic or equivalent isotropic displacement parameters (Å²)

	x	*y*	*z*	U_{iso}*/U_{eq}	Occ. (<1)
O1	0.77486 (11)	0.35341 (10)	0.589910 (18)	0.01462 (16)	
O2	0.75255 (11)	0.17812 (10)	0.534833 (18)	0.01484 (16)	
O3	0.09676 (11)	0.04131 (10)	0.605155 (16)	0.01295 (16)	
H3	0.018 (2)	0.1550 (14)	0.6051 (4)	0.0194*	
O4	0.20678 (12)	0.40123 (10)	0.641673 (17)	0.01535 (17)	
N1	0.28382 (13)	0.13325 (12)	0.537229 (19)	0.01340 (18)	
H1a	0.301 (2)	0.2103 (18)	0.5158 (2)	0.0161*	
H1b	0.346 (2)	0.0042 (13)	0.5315 (3)	0.0161*	
H1c	0.1276 (12)	0.130 (2)	0.5419 (3)	0.0161*	
C1	0.66400 (15)	0.25824 (12)	0.56411 (2)	0.0113 (2)	
C2	0.39707 (15)	0.23551 (12)	0.57080 (2)	0.0099 (2)	
H2	0.333017	0.381264	0.574629	0.0119*	
C3	0.33896 (14)	0.10323 (13)	0.60703 (2)	0.0105 (2)	
C4	0.48580 (15)	−0.09801 (13)	0.60976 (2)	0.0153 (2)	
H4a	0.425849	−0.186142	0.630443	0.023*	
H4b	0.475092	−0.176071	0.585871	0.023*	
H4c	0.650907	−0.061281	0.614737	0.023*	
C5	0.37622 (15)	0.23453 (13)	0.64294 (2)	0.0123 (2)	
H5a	0.346807	0.145323	0.665499	0.0148*	
H5b	0.537358	0.295211	0.642808	0.0148*	
C6	0.19156 (15)	0.53282 (13)	0.67244 (2)	0.0129 (2)	
C7	0.36283 (16)	0.54550 (14)	0.70072 (2)	0.0159 (2)	
H7	0.497301	0.455716	0.700158	0.0191*	
C8	0.33347 (18)	0.69234 (16)	0.72989 (3)	0.0210 (2)	
H8	0.449345	0.702075	0.749283	0.0252*	
C9	0.13815 (18)	0.82407 (16)	0.73102 (3)	0.0224 (3)	
H9	0.120233	0.92349	0.750999	0.0268*	
C10	−0.03148 (18)	0.80945 (15)	0.70263 (3)	0.0201 (2)	
H10	−0.165263	0.900049	0.703217	0.0241*	
C11	−0.00726 (16)	0.66341 (13)	0.67335 (3)	0.0165 (2)	
H11	−0.124654	0.652721	0.654204	0.0197*	
O5	0.98748 (13)	0.69494 (11)	0.559084 (18)	0.02150 (18)	
H5c	0.931 (3)	0.5734 (12)	0.5719 (3)	0.0323*	
H5d	1.016 (3)	0.7963 (14)	0.5786 (2)	0.0323*	
O6	1.0256 (5)	0.7611 (3)	0.48073 (5)	0.0180 (3)	0.6241
H6a	1.176 (2)	0.737 (5)	0.4691 (6)	0.027*	0.6241
H6b	1.055 (4)	0.754 (5)	0.50732 (14)	0.027*	0.6241
O7	0.893 (3)	0.7926 (14)	0.4836 (3)	0.0257 (5)	0.3759
H7a	0.750 (6)	0.859 (11)	0.4754 (16)	0.0386*	0.3759
H7b	0.873 (11)	0.776 (8)	0.5104 (4)	0.0386*	0.3759

Atomic displacement parameters (Å²)

	U^{11}	U^{22}	U^{33}	U^{12}	U^{13}	U^{23}
O1	0.0111 (3)	0.0142 (3)	0.0186 (3)	−0.0031 (2)	−0.0028 (2)	0.0001 (2)

O2	0.0105 (3)	0.0181 (3)	0.0159 (3)	0.0008 (2)	0.0019 (2)	0.0011 (2)
O3	0.0084 (3)	0.0128 (3)	0.0176 (3)	−0.0019 (2)	−0.0004 (2)	0.0014 (2)
O4	0.0155 (3)	0.0178 (3)	0.0128 (3)	0.0052 (2)	−0.0029 (2)	−0.0033 (2)
N1	0.0099 (3)	0.0191 (3)	0.0112 (3)	−0.0006 (3)	−0.0008 (2)	−0.0015 (2)
C1	0.0095 (4)	0.0093 (4)	0.0152 (4)	−0.0002 (3)	−0.0002 (3)	0.0030 (3)
C2	0.0084 (4)	0.0104 (3)	0.0110 (3)	0.0002 (3)	−0.0015 (3)	0.0000 (3)
C3	0.0089 (4)	0.0105 (3)	0.0120 (3)	−0.0009 (3)	−0.0008 (3)	0.0007 (3)
C4	0.0132 (4)	0.0116 (4)	0.0211 (3)	0.0011 (3)	−0.0019 (3)	0.0031 (3)
C5	0.0108 (4)	0.0142 (4)	0.0120 (3)	0.0009 (3)	−0.0017 (3)	0.0002 (3)
C6	0.0145 (4)	0.0132 (4)	0.0110 (3)	−0.0028 (3)	0.0018 (3)	0.0006 (3)
C7	0.0159 (4)	0.0187 (4)	0.0132 (4)	0.0000 (3)	−0.0010 (3)	−0.0005 (3)
C8	0.0228 (5)	0.0248 (4)	0.0154 (4)	−0.0033 (4)	−0.0031 (3)	−0.0035 (3)
C9	0.0286 (5)	0.0194 (4)	0.0190 (4)	−0.0020 (4)	0.0030 (4)	−0.0065 (3)
C10	0.0214 (4)	0.0184 (4)	0.0204 (4)	0.0020 (3)	0.0050 (3)	−0.0016 (3)
C11	0.0167 (4)	0.0175 (4)	0.0151 (4)	0.0006 (3)	0.0002 (3)	0.0002 (3)
O5	0.0255 (4)	0.0197 (3)	0.0193 (3)	−0.0088 (3)	0.0026 (2)	−0.0023 (2)
O6	0.0130 (6)	0.0234 (4)	0.0175 (4)	−0.0014 (3)	0.0000 (3)	−0.0045 (3)
O7	0.0226 (12)	0.0314 (7)	0.0232 (6)	0.0032 (6)	−0.0010 (5)	−0.0088 (5)

Geometric parameters (Å, º)

	Average	Minimum	Maximum
O1—C1	1.259 (5)	1.257 (5)	1.262 (5)
O2—C1	1.255 (3)	1.254 (4)	1.256 (4)
O3—H3	0.848 (13)	0.835 (14)	0.863 (14)
O3—C3	1.43 (2)	1.43 (2)	1.43 (2)
O4—C5	1.427 (10)	1.425 (11)	1.428 (11)
O4—C6	1.3704 (14)	1.3688 (14)	1.3718 (14)
N1—H1a	0.906 (13)	0.901 (13)	0.911 (13)
N1—H1b	0.912 (12)	0.893 (12)	0.931 (12)
N1—H1c	0.901 (17)	0.900 (17)	0.901 (17)
N1—C2	1.494 (5)	1.494 (5)	1.495 (5)
C1—C2	1.54 (2)	1.53 (2)	1.54 (2)
C2—H2	1.000 (2)	1.000 (2)	1.000 (2)
C2—C3	1.5629 (19)	1.5605 (19)	1.5645 (19)
C3—C4	1.523 (7)	1.521 (8)	1.526 (8)
C3—C5	1.5297 (16)	1.5281 (16)	1.5317 (16)
C4—H4a	0.980 (2)	0.979 (2)	0.981 (2)
C4—H4b	0.9800 (12)	0.9787 (12)	0.9813 (12)
C4—H4c	0.980 (14)	0.979 (14)	0.981 (14)
C5—H5a	0.9900 (12)	0.9896 (12)	0.9904 (12)
C5—H5b	0.990 (13)	0.990 (13)	0.990 (13)
C6—C7	1.394 (11)	1.393 (11)	1.395 (11)
C6—C11	1.397 (14)	1.396 (14)	1.397 (14)
C7—H7	0.950 (10)	0.950 (10)	0.950 (10)
C7—C8	1.3960 (19)	1.3950 (19)	1.3969 (19)
C8—H8	0.950 (7)	0.950 (7)	0.950 (7)
C8—C9	1.385 (14)	1.383 (14)	1.388 (14)

C9—H9	0.9500 (15)	0.9500 (16)	0.9500 (16)
C9—C10	1.391 (10)	1.390 (11)	1.392 (11)
C10—H10	0.950 (9)	0.950 (9)	0.950 (9)
C10—C11	1.3923 (19)	1.3898 (19)	1.3949 (19)
C11—H11	0.950 (7)	0.950 (7)	0.950 (7)
O5—H5c	0.958 (13)	0.946 (15)	0.968 (15)
O5—H5d	0.958 (11)	0.952 (12)	0.963 (12)
O6—H6a	0.96 (2)	0.96 (3)	0.96 (3)
O6—H6b	0.957 (9)	0.955 (12)	0.960 (12)
O7—H7a	0.96 (6)	0.96 (8)	0.96 (8)
O7—H7b	0.96 (3)	0.96 (3)	0.96 (3)
H3—O3—C3	105.7 (10)	104.7 (10)	106.9 (10)
C5—O4—C6	117.80 (10)	117.63 (10)	117.99 (10)
H1a—N1—H1b	104.7 (14)	103.0 (14)	106.5 (13)
H1a—N1—H1c	105.8 (15)	103.2 (15)	108.4 (15)
H1b—N1—H1c	113.7 (14)	111.5 (14)	115.9 (15)
H1a—N1—C2	112.5 (10)	111.5 (10)	113.5 (10)
H1b—N1—C2	113.3 (10)	111.2 (10)	115.3 (10)
H1c—N1—C2	106.6 (10)	106.3 (10)	107.1 (10)
O1—C1—O2	126.09 (13)	125.92 (13)	126.27 (13)
O1—C1—C2	115.09 (10)	115.01 (10)	115.18 (11)
O2—C1—C2	118.79 (11)	118.57 (11)	118.99 (11)
N1—C2—C1	109.93 (9)	109.83 (9)	110.04 (9)
N1—C2—H2	110.52	110.43	110.6
N1—C2—C3	109.06 (9)	108.94 (9)	109.15 (9)
C1—C2—H2	106.94	106.68	107.23
C1—C2—C3	112.49 (9)	112.22 (9)	112.73 (9)
H2—C2—C3	107.86	107.75	107.99
O3—C3—C2	108.14 (9)	107.96 (9)	108.34 (9)
O3—C3—C4	107.34 (9)	107.25 (9)	107.41 (9)
O3—C3—C5	108.64 (10)	108.60 (10)	108.68 (10)
C2—C3—C4	112.59 (9)	112.47 (9)	112.71 (9)
C2—C3—C5	110.97 (9)	110.85 (9)	111.09 (9)
C4—C3—C5	109.03 (9)	108.88 (9)	109.19 (9)
C3—C4—H4a	109.47	109.45	109.5
C3—C4—H4b	109.47	109.45	109.49
C3—C4—H4c	109.47	109.41	109.54
H4a—C4—H4b	109.47	109.46	109.48
H4a—C4—H4c	109.47	109.43	109.52
H4b—C4—H4c	109.47	109.45	109.49
O4—C5—C3	106.43 (10)	106.28 (10)	106.60 (10)
O4—C5—H5a	109.47	109.46	109.48
O4—C5—H5b	109.47	109.46	109.48
C3—C5—H5a	109.47	109.47	109.48
C3—C5—H5b	109.47	109.45	109.5
H5a—C5—H5b	112.35	112.22	112.5
O4—C6—C7	123.93 (12)	123.73 (12)	124.12 (12)

O4—C6—C11	115.34 (11)	115.20 (11)	115.48 (11)
C7—C6—C11	120.69 (11)	120.59 (11)	120.79 (11)
C6—C7—H7	120.56	120.47	120.64
C6—C7—C8	118.89 (13)	118.72 (13)	119.06 (13)
H7—C7—C8	120.55	120.47	120.64
C7—C8—H8	119.46	119.41	119.5
C7—C8—C9	121.08 (14)	120.99 (14)	121.17 (14)
H8—C8—C9	119.46	119.41	119.5
C8—C9—H9	120.3	120.28	120.33
C8—C9—C10	119.39 (14)	119.34 (14)	119.44 (14)
H9—C9—C10	120.3	120.28	120.33
C9—C10—H10	119.66	119.64	119.67
C9—C10—C11	120.68 (14)	120.65 (14)	120.71 (14)
H10—C10—C11	119.66	119.65	119.67
C6—C11—C10	119.26 (13)	119.24 (13)	119.28 (13)
C6—C11—H11	120.37	120.36	120.38
C10—C11—H11	120.37	120.36	120.38
H5c—O5—H5d	104.2 (11)	102.1 (11)	105.9 (11)
H6a—O6—H6b	105 (2)	104 (2)	105 (2)
H7a—O7—H7b	104 (7)	104 (7)	105 (6)

O1—C1—C2—N1	176.27 (9)	175.91 (9)	176.63 (9)
O1—C1—C2—C3	-61.99 (12)	-62.41 (12)	-61.57 (12)
O2—C1—C2—N1	-5.59 (14)	-6.00 (14)	-5.18 (14)
O2—C1—C2—C3	116.15 (11)	115.56 (11)	116.75 (11)
O3—C3—C5—O4	-53.93 (11)	-54.76 (11)	-53.11 (11)
O4—C6—C7—C8	177.16 (12)	176.58 (12)	177.74 (12)
O4—C6—C11—C10	-176.93 (11)	-177.57 (11)	-176.29 (11)
N1—C2—C3—O3	-41.85 (11)	-43.40 (11)	-40.32 (11)
N1—C2—C3—C4	76.57 (11)	74.87 (11)	78.26 (11)
N1—C2—C3—C5	-160.91 (9)	-162.36 (10)	-159.46 (10)
C1—C2—C3—O3	-164.09 (9)	-165.90 (8)	-162.28 (9)
C1—C2—C3—C4	-45.67 (12)	-47.64 (12)	-43.70 (12)
C1—C2—C3—C5	76.85 (11)	75.14 (12)	78.57 (11)
C2—C3—C5—O4	64.83 (12)	63.76 (12)	65.89 (12)
C4—C3—C5—O4	-170.60 (9)	-171.44 (9)	-169.76 (9)
C5—O4—C6—C7	15.18 (17)	13.15 (17)	17.21 (17)
C5—O4—C6—C11	-167.03 (11)	-169.23 (11)	-164.84 (11)
C6—O4—C5—C3	175.01 (10)	173.67 (10)	176.37 (10)
C6—C7—C8—C9	0.01 (14)	-0.1 (2)	0.1 (2)
C7—C6—C11—C10	0.93 (19)	0.34 (19)	1.52 (19)
C7—C8—C9—C10	0.1 (2)	-0.3 (2)	0.4 (2)
C8—C9—C10—C11	0.3 (2)	0.0 (2)	0.6 (2)
C9—C10—C11—C6	-0.8 (2)	-1.1 (2)	-0.6 (2)
C11—C6—C7—C8	-0.51 (17)	-1.01 (19)	0.00 (18)